Absorption and luminescence spectroscopy of transition metal compounds: from coordination geometries to excited-state properties [1]

Christian Reber*

Département de chimie, Université de Montréal, Montréal QC H3C 3J7, Canada.

Received: April 14, 2008 Accepted (in revised form): April 30, 2008

Abstract

Absorption spectra of transition metal compounds provide important experimental information for the understanding of their chemistry. The combination with luminescence spectra yields quantitative insight on excited-state properties, in particular from spectra with resolved vibronic structure measured at low temperature. Three categories of complexes are used to illustrate how their electronic structure can be characterized in detail. The first examples are aquo complexes of first row d-block metal ions with absorption spectra showing interference dips, the second category are trans-dioxo rhenium(V) complexes with metal-ligand single and double bonds leading to luminescence spectra with characteristic vibronic structure, and finally square-planar complexes of palladium(II) and platinum(II) with large changes of luminescence intensities and wavelengths induced by external pressure are presented.

Keywords*:* absorption spectroscopy, luminescence spectroscopy, transition metal complexes, award lecture, review

Résumé

Les spectres d'absorption des composés des éléments de transition sont d'importance primordiale pour la caractérisation de leurs structures et liaisons chimiques. La combinaison de spectres d'absorption et de luminescence mène à des informations quantitatives sur les états électroniques excités, surtout si les spectres montrent de la structure vibronique résolue, ce qui est régulièrement le cas pour des mesures effectuées à basse température. Trois catégories de complexes métalliques sont utilisées pour illustrer l'application de ces techniques spectroscopiques. Le premier groupe sont des complexes aquo d'ions de la série 3d avec des spectres d'absorption qui montrent des creux d'interférence. Les composés de la deuxième série, des complexes trans-dioxo du rhénium(V), ont des spectres de luminescence avec des patrons de pics vibroniques caractéristiques, déterminés par les liaisons métal-ligand simples et multiples. La dernière famille sont les complexes de structure plan-carrée du palladium(II) et du platine(II) qui montrent des grands changements de leurs intensités et longueurs d'onde de luminescence sous l'influence d'une pression externe.

Introduction

One of the most easily perceptible aspects of coordination chemistry is the variety of colors that are observed for many transition metal complexes and organometallic molecules [2]. These colors are a visual manifestation of quantum mechanics and are determined by the electronic structure of the compounds [3-5]. Absorption and luminescence spectra in the visible wavelength range provide quantitative measurements [6-8] of color and have been used to characterize the structure and bonding of these molecules in the electronic ground state. Spectra also provide detailed information on electronic excited states of key importance for photochemistry [9-11] and for a variety of optical materials properties [12,13]. Often, advanced variants of luminescence and absorption spectroscopy [14] or other techniques, such as resonance

*Author to whom correspondence should be addressed: e-mail: christian.reber@umontreal.ca (Christian Reber)

Raman [15-18] or electron paramagnetic resonance spectroscopy [19], are combined with absorption and luminescence measurements to advance our knowledge of intriguing chemical systems involving a wide variety of transition metal compounds.

In this overview, example spectra are used to illustrate the quantitative insight that can be obtained from absorption and luminescence spectra, in combination with models that go beyond purely electronic aspects, such as those used for traditional ligand field or molecular orbital diagrams that always imply artificially "frozen" structures, i.e. no molecular structure changes for different electron configurations and electronic states [5,20,21]. Experimental spectra involve both electronic and vibronic transitions, and often several different intensity mechanisms contribute to a single band [7,8,22], emphasizing that purely electronic models are not adequate.

Potential energy surfaces provide a more appropriate quantitative approach to the understanding of absorption and luminescence spectra. A simple model limited to two electronic states is shown in Figure 1. It involves only a single normal coordinate Q_i, defined here in dimensionless units, and harmonic potential energy curves with identical vibrational frequencies, given throughout this overview in cm^{-1} (wavenumber) units, are used to describe both the ground state and the only excited state. The transition is assumed to be allowed with a transition dipole whose magnitude does not vary along the normal coordinate Q_i. The ground state equilibrium geometry corresponds to the origin of the normal coordinate axis, and the ground-state potential energy curve is defined by experimental vibrational frequencies. Energy differences between the two potential energy curves can be determined from absorption and luminescence spectra, as illustrated on the right-hand side of Figure 1. The electronic origin transition denoted by E_{00} occurs between the lowest-energy vibrational levels of the two electronic states. These levels are shown in Figure 1, and the energy of the electronic origin is identical in absorption and luminescence spectra. Luminescence and absorption band maxima correspond to vertical transitions, shown as solid and dotted arrows in Figure 1. The band maxima are separated by the Stokes shift, also illustrated in Figure 1.

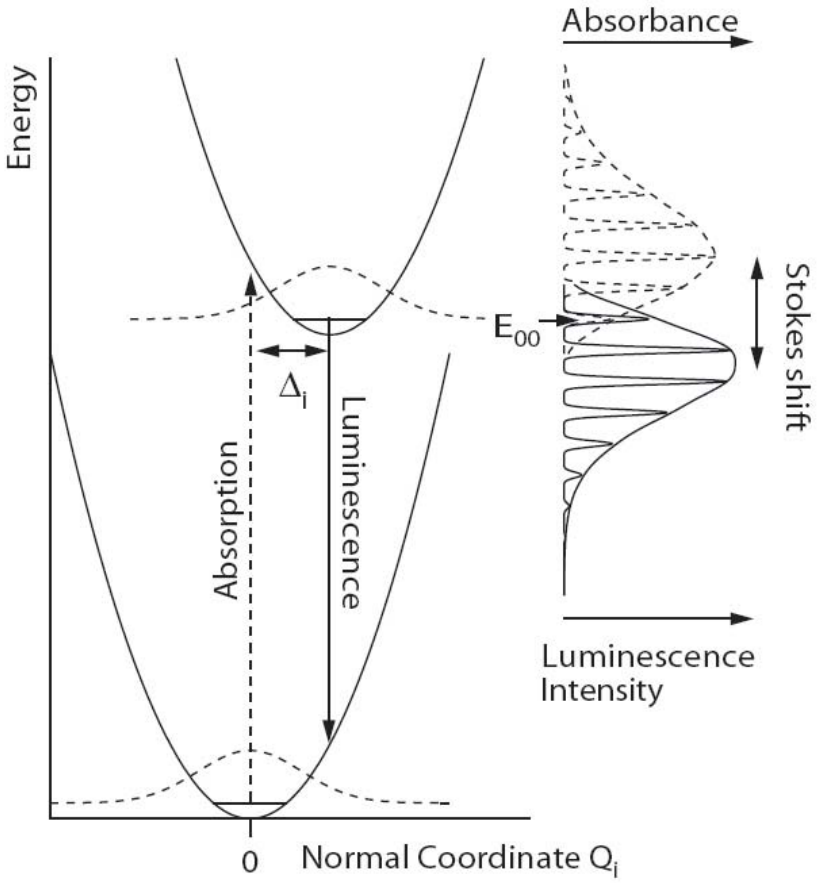

Figure 1. Potential energy curves of the electronic ground state and a single excited state along one normal coordinate Q_i. Solid and dotted arrows denote luminescence and absorption band maxima. The lowest-energy vibrational eigenfunctions of both potential energy curves are given as dotted traces. Calculated absorption and luminescence spectra with resolved vibronic structure are shown as dotted and solid lines, respectively, with the electronic origin E_{00} and the Stokes shift indicated. Unresolved spectra define the envelope of the spectra with resolved vibronic progressions.

Broad absorption and luminescence bands are observed if a significant structural change, corresponding to a sizable offset Δ_i in Figure 1, occurs along at least one normal coordinate Q_i [15,23,24]. These offsets cause the large bands usually observed in the spectra of transition metal compounds in solution at room temperature.

Many spectra of crystalline compounds measured at low temperature show resolved vibronic structure, allowing a quantitative comparison between experimental and calculated spectra. The model in Figure 1 leads to a single vibronic progression in luminescence and absorption spectra with intervals corresponding to ground- and excited-state vibrational frequencies. The harmonic potential energy curves are a special case leading to identical calculated spectra for offsets $\pm\Delta_i$. Coordinates with nonzero offsets Δ_i can be identified from spectra with resolved vibronic structure, as illustrated by the calculated spectra in Figure 1. The fit of calculated spectra to experimental data leads to numerical values of all parameters necessary to define the model in Figure 1, most notably the magnitudes of the structural differences Δ_i between the ground and excited states, key quantities defining photochemical properties. Values for Δ_i have been determined from absorption, luminescence and resonance Raman spectra for many compounds [18,25-27]. Calculations based on the model in Figure 1 are easily carried out [24,28-30]. We use the time-dependent theory of spectroscopy, [15,23,31] as it can be generalized to models beyond the simple case shown in Figure 1 and because it provides intuitive insight. Recently, detailed potential energy surfaces obtained from advanced electronic structure calculations have been compared to experimental spectra, [32-36] a very promising research area providing new knowledge on electronic structure beyond the traditional assumption of "frozen" structures.

Colors of transition metal complexes: the absorption spectrum of $Ni(H_2O)_6^{2+}$

Many colored transition metal complexes are easily synthesized and the understanding of the structural and electronic factors defining their color is at the center of well-established undergraduate-level laboratory experiments [37-40]. A popular category of transition metal complexes used to illustrate the effect of metal-ligand bond strengths on spectra are octahedral nickel(II) complexes with the d^8 electron configuration. Figure 2 shows two typical complexes, $[Ni(H_2O)_6]^{2+}$ and $[Ni(NH_3)_6]^{2+}$, and their absorption spectra measured in solution at room temperature. The spectra show broad bands with widths at half height on the order of 3000 cm^{-1}, indicative of significant structure changes between the initial and final states of the absorption transition and therefore nonzero values of Δ_i, as illustrated in Figure 1. Both spectra show three broad bands with molar absorptivities ε of less than 10 $M^{-1}cm^{-1}$, typical for parity-forbidden d-d transitions of octahedral complexes [4,8]. Relatively small wavelength changes of the absorption bands lead to the easily perceived color differences of the solutions shown in Figure 2. Energies of band maxima are higher for $[Ni(NH_3)_6]^{2+}$ than for $[Ni(H_2O)_6]^{2+}$, a trend corresponding to the spectrochemical series [20]. An intriguing spectroscopic feature is the middle band of the $[Ni(H_2O)_6]^{2+}$ complex. This is by far the largest band in Figure 2, its width at half height of almost 4000 cm^{-1} is indicated by the horizontal double arrow. The band shows two maxima, separated by the interference dip [41-45] marked by an asterisk in Figure 2. The analysis of this absorption band system has a long and controversial history [46-50]. It arises from coupling between two excited states of different multiplicity close in energy, leading to interference between two transitions, a situation beyond the model in Figure 1 with only a single excited state, but straightforward to analyze from the time-dependent viewpoint [41-43,50].

Figure 3 shows an enlarged view of the middle band of a related nickel(II) complex, *trans*-$[NiCl_2(H_2O)_4]\cdot 2H_2O$ [50,51]. The spectrum was measured with a single crystal sample at low temperature and shows well-resolved vibronic structure, in contrast to the unresolved bands in the room-temperature solution spectra in Figure 1. The point group symmetry of this complex is D_{4h}, and significantly different spectra are observed with σ and π polarized light, as the fourfold molecular axes of all complexes are parallel in this crystal structure. In this lower symmetry, some degeneracies of electronic states in O_h point group symmetry are lifted, leading to doubled patterns, such as those indicated by the vertical markers for the π polarized spectrum in Figure 3, but the deviations from octahedral symmetry are small, as the two different ligands have similar strengths. The detailed vibronic patterns confirm the assignment as arising from an interference dip. Spectra with interference dips can be calculated from models based on coupled potential energy surfaces along a single totally symmetric normal coordinate, leading to the excellent agreement between experimental and calculated spectra of *trans*-$[NiCl_2(H_2O)_4]\cdot 2H_2O$ in Figure 3 and for a number of other compounds [43,52]. The calculated spectra yield values for Δ_i and for the magnitude of coupling between excited states, and the

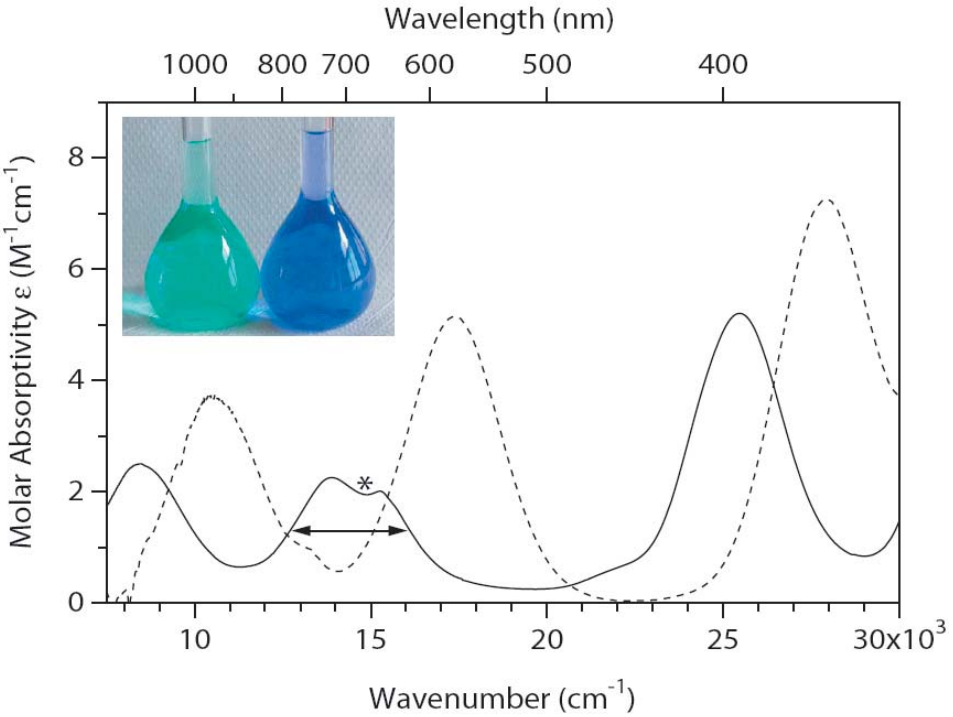

Figure 2. Absorption spectra of $[Ni(H_2O)_6]^{2+}$ and $[Ni(NH_3)_6]^{2+}$ in aqueous solution. The photograph shows the characteristic green and blue colors of $[Ni(H_2O)_6]^{2+}$ and $[Ni(NH_3)_6]^{2+}$, respectively. The horizontal double-headed arrow identifies the unusually large middle band in the spectrum of $[Ni(H_2O)_6]^{2+}$ and the asterisk denotes the interference dip observed on this band.

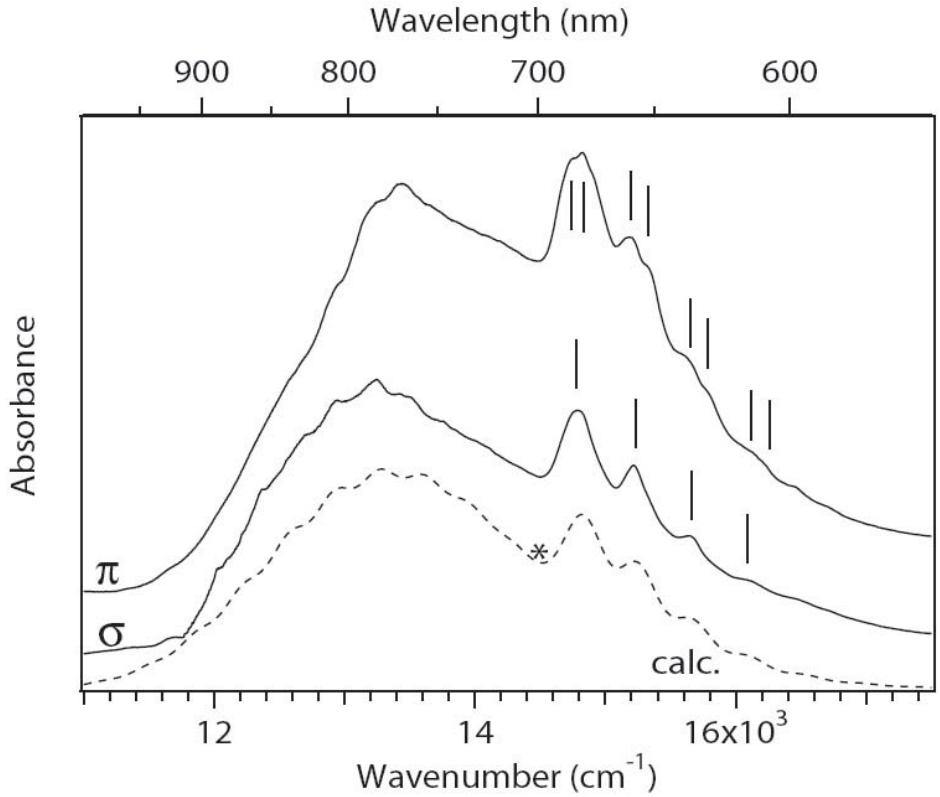

Figure 3. Polarized single-crystal spectra of *trans*-$[NiCl_2(H_2O)_4]\cdot 2H_2O$ measured at 5 K. Only the middle band of the spectra is shown. The dotted trace denotes a calculated spectrum based on coupled potential energy curves involving multiple excited states. Vertical markers indicate band maxima and emphasize the differences observed in σ and π polarizations. The interference dip is denoted by the asterisk on the calculated spectrum.

time-dependent theory clearly shows the physical origin of the interference dip [41-43]. The absorption spectra in Figure 3 illustrate the detailed information that can be obtained from spectra with resolved vibronic structure. Absorption spectra with forbidden bands close in energy to several allowed transitions show intensities determined by more complicated constructive or destructive interference effects [52] and have yet to be studied in detail for transition metal compounds.

Figure 4 shows absorption and luminescence spectra of $Cs_2[CrCl_2(H_2O)_4]Cl_3$ measured at 5 K [51,53]. These crystals contain tetragonal *trans*-$[CrCl_2(H_2O)_4]^+$ chromophores with D_{4h} point group symmetry, identical to the nickel(II) analog discussed in the preceding paragraph. The spectra in Figure 4 show a well resolved electronic origin observed at identical energy in absorption and luminescence spectra, a clear experimental example for this aspect of Figure 1. The symmetry of the excited state can be unambiguously assigned from the polarization of the absorption transition. The origin is only allowed through the magnetic dipole intensity mechanism, but the main intensity of the bands arises through electric dipole, vibronic mechanisms. The inset to Figure 4 shows the negligible contribution of the electronic origin and its vibronic progressions to the overall intensity of the lowest-energy spin-allowed transition. Calculated spectra are therefore usually based on values of E_{00} that correspond to vibronic origins, even if the true electronic origin can be observed. The spectra in Figure 4 show that vibronic structure varying in intensity by several orders of magnitude can be measured precisely, an essential prerequisite for the characterization of many transition metal compounds.

Metal-oxo multiple bonds: luminescence spectra with resolved vibronic structure

This section focuses on luminescence and absorption spectra of six-coordinate transition metal complexes with formally different metal-ligand bond orders. We use a series of well –known *trans*-dioxo rhenium(V) complexes

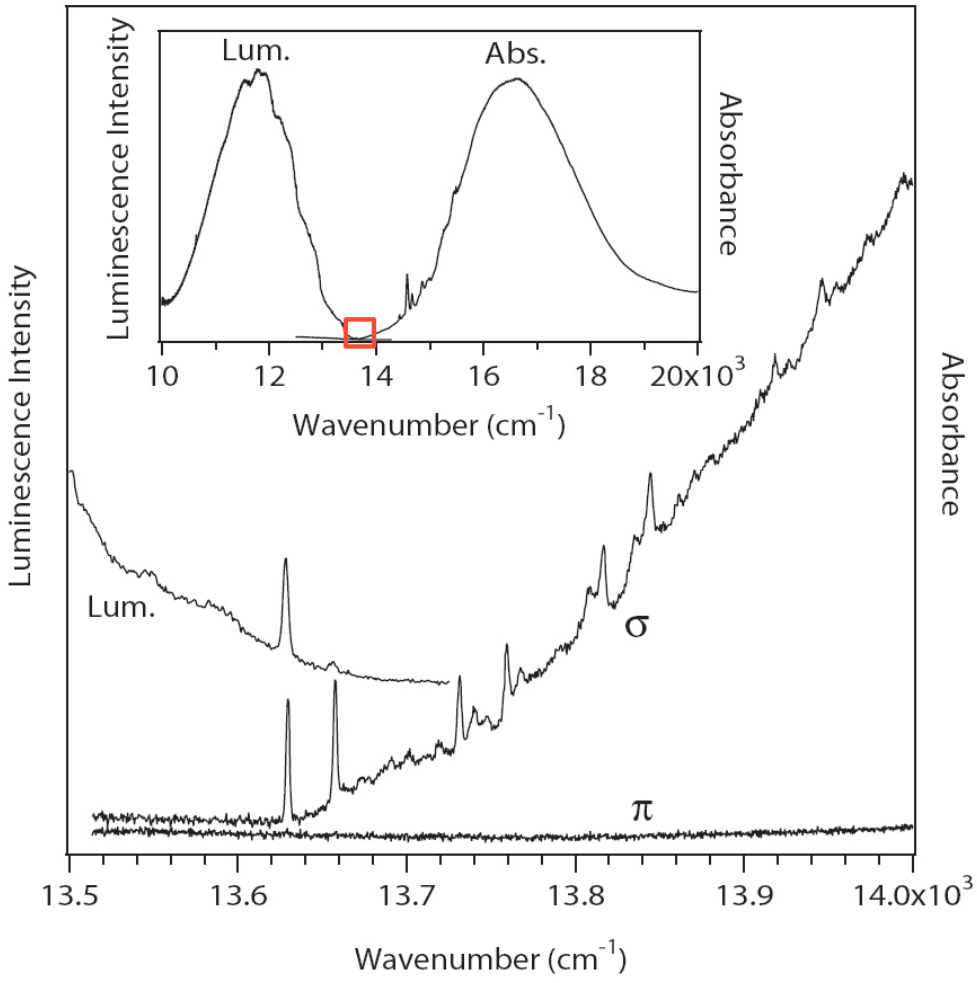

Figure 4. Single-crystal absorption and luminescence spectra of $Cs_2[CrCl_2(H_2O)_4]Cl_3$. All spectra were measured at 5 K. The main Figure shows the region of the electronic origins, observed both in the σ-polarized absorption and unpolarized luminescence spectra, given as the middle and top traces, respectively. The inset shows the lowest-energy spin-allowed transition, with the origin area denoted by the rectangle enlarged in the main Figure .

as illustrative examples. These complexes have the d^2 electron configuration and a totally symmetric singlet ground state. Their spectroscopic and photochemical properties have been studied in detail [54-62]. Each complex contains two rhenium-oxo multiple bonds and four single bonds to ancillary ligands and has idealized D_{4h} point group symmetry. Many crystal structures have been reported, and the difference between single and multiple bond lengths is on the order of 0.3 Å, a very significant deviation from octahedral symmetry.

Figure 5 shows absorption and luminescence spectra of the *trans*-$[ReO_2(ethylenediamine)_2]^+$ complex. The solution absorption spectrum has two weak bands in the visible wavelength range, assigned as d-d transitions to the lowest-energy triplet and singlet excited states [58,60]. These transitions involve states with electron configurations arising from the octahedral $(t_{2g})^2$ manifold, illustrating the large energy separation of this triply degenerate ensemble of orbitals in the D_{4h} point group symmetry of six-coordinate complexes with different metal-ligand bond orders. The low-temperature spectra of single crystalline *trans*-$[ReO_2(ethylenediamine)_2]Cl$ show resolved vibronic structure involving the high-frequency symmetric Re-oxo stretching mode with frequency $\hbar\omega_{O=Re=O}$ and the lower-frequency Re-ancillary ligand mode with frequency $\hbar\omega_{Re-N}$. The spectra allow a comparison of the ground- and excited state vibrational frequencies of these two modes. The Re-oxo frequency decreases by approximately 100 cm^{-1} in the excited state. In contrast, the Re-ethylenediamine frequency increases by 50 cm^{-1} in the excited state. The decrease of $\hbar\omega_{O=Re=O}$ indicates weaker Re-oxo bonds in the excited state, the increase of $\hbar\omega_{Re-N}$ is indicative of stronger Re-ancillary ligand bonds in the emitting state. This comparison is strong evidence for offsets $\Delta_{O=Re=O}$ and Δ_{Re-N} with different signs, overcoming the intrinsic limitation of harmonic potential energy curves to absolute values $|\Delta_i|$. Significant structural changes Δ_i occur along the normal coordinates of both modes, and models as illustrated in Figure 1 have been applied to quantitatively determine these changes [57,58].

Figure 6 shows low-temperature luminescence spectra of *trans*-dioxo rhenium(V) complexes with pyridine and imidazole ancillary ligands. The observed lumines-

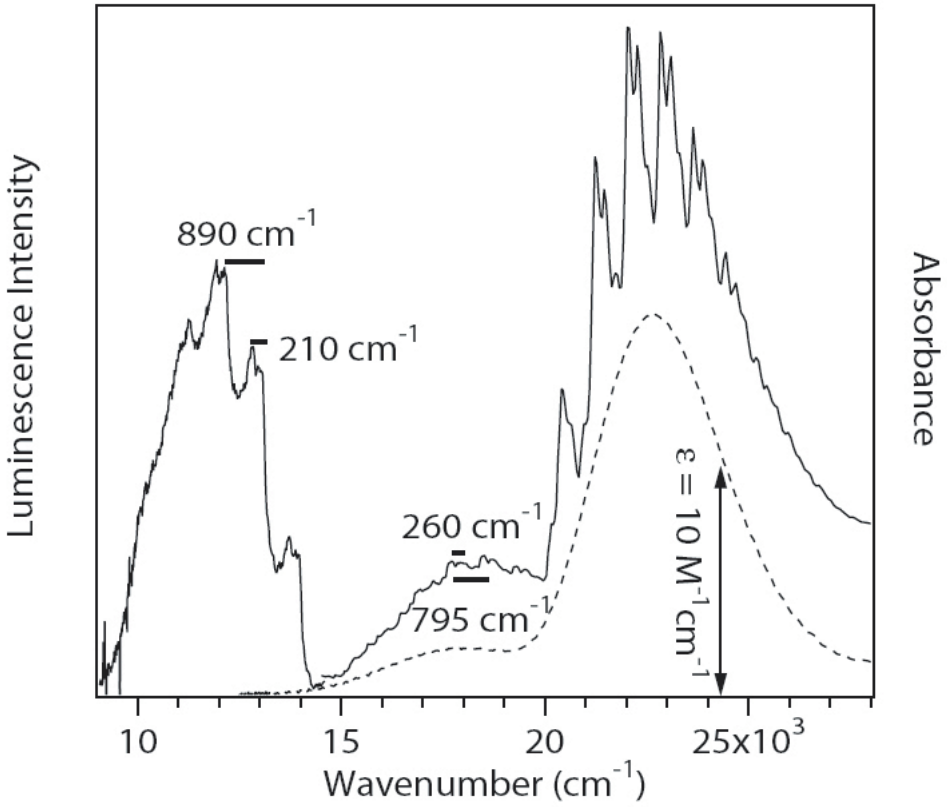

Figure 5. Absorption and luminescence spectra of *trans*-$[ReO_2(en)_2]^+$. The solution absorption spectrum measured at room temperature is shown as a dotted trace, with a molar absorptivity scale given. Crystal spectra of *trans*-$[ReO_2(en)_2]Cl$ measured at 15 K are shown as solid traces. Ground- and excited-state vibrational frequencies determined from the resolved vibronic intervals are given.

cence maximum is higher in energy by approximately 3000 cm^{-1} for *trans*-[ReO_2(pyridine)$_4$]I [55] than for *trans*-[ReO_2(1-methylimidazole)$_4$]I [57,59]. Vibronic progressions involving both the Re-oxo and Re-ancillary modes can easily be identified. A calculated spectrum based on two-dimensional harmonic potential energy surfaces defined along the normal coordinates of these two modes is in very good agreement with the experimental data and precise absolute values $|\Delta_i|$ can be obtained, as summarized in Table 1. The model based on harmonic potential energy surfaces leads to a calculated spectrum that reproduces the overall patterns and intensity distributions for *trans*-[ReO_2(1-methylimidazole)$_4$]I well, but fails to reproduce an essential experimental feature. The intensity distribution within each "cluster" of peaks varies systematically across the spectrum, as indicated by the sloped lines in Figure 6, and in a similar manner across the luminescence spectrum in Figure 5. This variation indicates coupling between the two normal coordinates, arising from coupling with excited states, and a model including these effects leads to a calculated spectrum reproducing the experimental intensity variations, as shown by the top dotted trace in Figure 6 [57,59]. The effect becomes stronger if the energy difference between the ground and excited states decreases, and it is therefore observed in the low-energy luminescence spectra, but not in the higer-energy luminescence spectrum of *trans*-[ReO_2(pyridine)$_4$]I, whose vibronic intensities are perfectly reproduced by the calculation based on harmonic potential energy surfaces, as shown by the bottom traces in Figure 6. These luminescence spectra illustrate the unique level of quantitative detail that can be obtained, in particular by comparing series of related compounds [57,59].

The luminescence spectra in Figure 6 retain some resolution at higher temperature, as illustrated in the inset to the Figure. These spectra no longer show distinct vibronic intervals for two progressions, but they can be perfectly reproduced for many compounds [25,55] by the parameters derived for the low-temperature spectra by simply increasing the vibronic line width Γ, given in Table 1 for the two compounds compared in Figure 6. The less-resolved spectra in the inset can also be analyzed by a model based on only one normal coordinate, exactly as shown in Figure 1. The calculated spectra are in excellent agreement with the experiments, as shown in the inset to

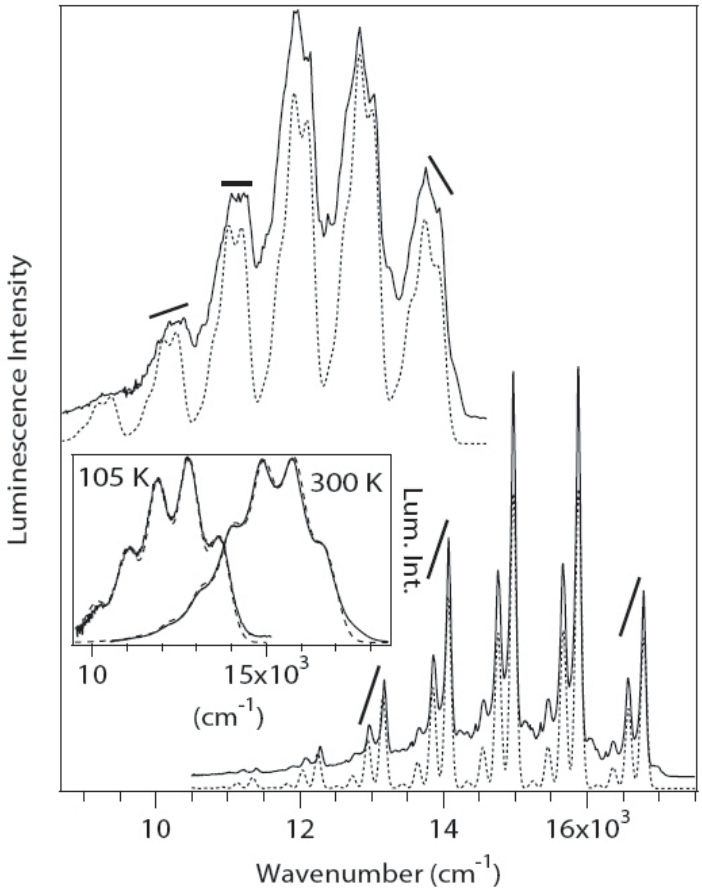

Figure 6. Low-temperature luminescence spectra of *trans*-[ReO_2(1-methylimidazole)$_4$]I (top, measured at 15 K) and *trans*-[ReO_2(pyridine)$_4$]I (bottom, measured at 5 K). Calculated spectra are given as dotted traces, with bars emphasizing differences in the vibronic intensity distributions of the two spectra. The inset shows luminescence spectra of *trans*-[ReO_2(1-methylimidazole)$_4$]I at 105 K and *trans*-[ReO_2(pyridine)$_4$]I at 300 K with calculated spectra given by dotted traces.

Figure 6, and the resulting parameters are summarized in Table 1. The observed vibronic interval $\hbar\omega_{MIME}$ has to be treated as an adjustable parameter, in contrast to the low-temperature spectra, where vibrational frequencies determined from Raman spectra were used to define the potential energy surfaces. The values for the high-temperature spectra in Table 1 do not correspond to an observed vibrational frequency, and the spectra therefore show a missing mode effect (MIME), analyzed for many compounds in the literature and straightforward to understand from the time dependent theory of spectroscopy [25,26,63,64]. The offset Δ_{MIME} is similar in size to the offset $\Delta_{O=Re=O}$ as this large offset along the coordinate of the high-frequency mode determines the width of the luminescence bands.

Pressure tuning of luminescence properties for square-planar complexes of palladium(II) and platinum(II)

Square-planar complexes of the divalent group 10 metal ions nickel(II), palladium(II) and platinum(II) with the d^8 electron configuration are the most representative examples for this coordination geometry. Their photochemistry has been explored, [65] and the absorption and luminescence spectra of palladium(II) and platinum(II) complexes can be characterized in detail with the models described in the previous sections. Many square-planar complexes with halide or thiocyanate ligands show Jahn-Teller distortions along non-totally symmetric stretching and bending coordinates [66] in the emitting state [67-70]. In order to understand variations between different compounds of this class, it is intriguing to consider continuous variations of structure and bonding, in contrast to the discrete changes that occur through chemical changes such as ligand substitution reactions. An experimental approach to such continuous variations is provided by external pressure, leading to characteristic shifts of luminescence and absorption band maxima [71-76]. These shifts have often been interpreted with purely electronic models, but again the vibronic approach illustrated in Figure 1 leads to a more precise analysis based on the observed band shapes and is not limited to the band maxima. Modern microscope spectrometers with sensitive imaging detectors for weak signals have enabled us to measure the room-temperature luminescence from square-planar complexes of platinum(II) and palladium(II).

The interconfigurational d-d absorption and luminescence band maxima of many square-planar and octahedral complexes show a blue shift with pressure, due to the increase of electron density in the σ-antibonding LUMO orbitals, which are strongly destabilized as a consequence of small pressure-induced bond length decreases [71-73]. This is illustrated for $[Pd(SCN)_4](n\text{-}Bu_4N)_2$ in Figure 7, where a blue shift of +29 cm^{-1}/kbar is determined from the luminescence band maxima [77,78]. The most intriguing aspect of the spectra in Figure 7 is the large increase of the luminescence intensity with pressure. The observed intensity reflects the competition between radiative and nonradiative relaxation processes, and either an increase of the radiative rate or a decrease of the nonradiative relaxation rate can lead to an intensity increase. Luminescence lifetime measurements at different pressures identify the dominant process, and the lifetimes given in the inset to Figure 7 clearly show a marked increase between ambient pressure and

Table 1. Numerical parameter values used to calculate the luminescence spectra in Figure 6.

Parameter	*trans*-ReO_2(pyridine)$_4$I	trans-ReO_2(1-methylimidazole)$_4$I
Low temperature		
$\hbar\omega_{O=Re=O}$ (cm^{-1})	907	905
$\lvert\Delta_{O=Re=O}\rvert$	2.18	2.27
$\hbar\omega_{Re-N}$ (cm^{-1})	212	215
$\lvert\Delta_{Re-N}\rvert$	1.00	1.53
E_{00} (cm^{-1})	16786	14140
Γ (cm^{-1})	30	60
High temperature		
$\hbar\omega_{MIME}$ (cm^{-1})	880	883
E_{00} (cm^{-1})	16650	13630
Γ (cm^{-1})	245	215

20 kbar, indicative of a decrease of the nonradiative relaxation rate [77,78]. This result shows that the small structural changes induced by pressure are not identical for the ground and emitting states and can greatly affect relaxation processes, important for the development of efficient luminescent materials.

A very different behavior is observed for the square-planar $[Pt(SCN)_4]^{2-}$ luminophore as part of the trimetallic $\{Pt(SCN)_2[\mu\text{-}SCN)Mn(NCS)(bipy)_2]_2\}$ complex. Its pressure-dependent luminescence spectra are shown in Figure 8 [79]. The band maxima show a large red-shift of -99 cm^{-1}/kbar, as given in the inset and compared to $[Pt(SCN)_4](n\text{-}Bu_4N)_2$, [77] where a blue shift of +25 cm^{-1}, comparable in size to the palladium(II) analog in Figure 7, is observed. The surprising red shift discovered for the trimetallic complex is due to intermolecular interactions with neighboring C-H bonds, providing a very sensitive approach to measuring such interactions. This final example illustrates how luminescence spectroscopy involving metal centered transitions can even be used to probe intermolecular interactions. Square-planar complexes are particularly attractive for the investigation of many types of such interactions.

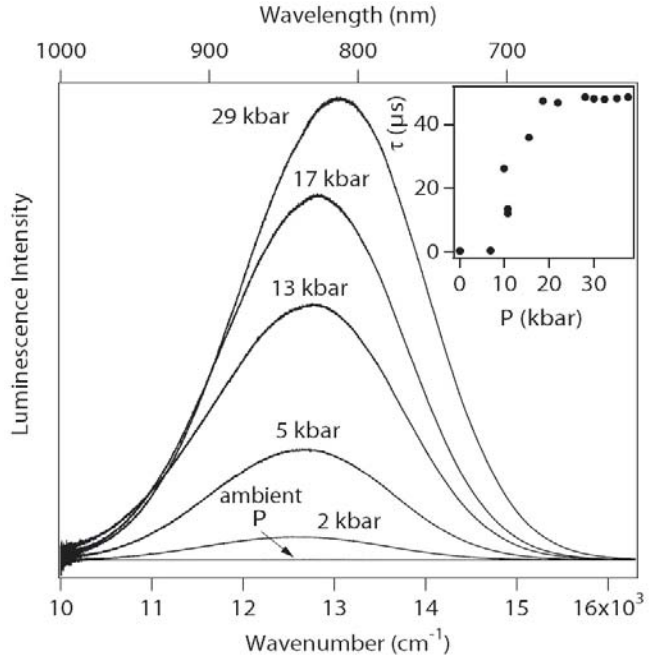

Figure 7. Luminescence spectra of $[Pd(SCN)_4](n\text{-}Bu_4N)_2$ as a function of external pressure. The inset shows pressure-dependent luminescence lifetimes. All measurements were made at room temperature.

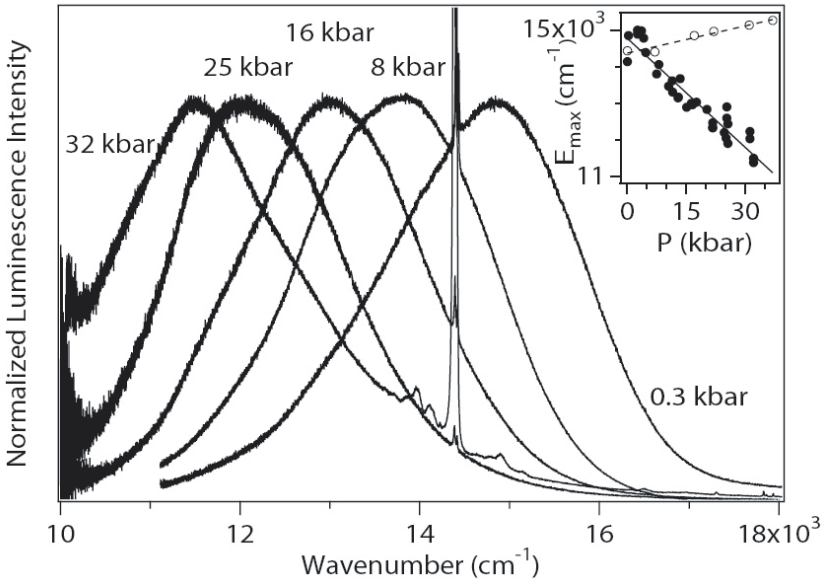

Figure 8. Luminescence spectra of the trimetallic complex $\{Pt(SCN)_2[\mu\text{-}SCN)Mn(NCS)(bipy)_2]_2\}$ at different pressures. One spectrum contains prominent ruby R-line luminescence at approximately 14400 cm^{-1}, used for pressure calibration. The inset shows variations of the luminescence maxima as a function of pressure by -99 cm^{-1}/kbar (solid line) and +25 cm^{-1}/kbar (dotted line) for $\{Pt(SCN)_2[\mu\text{-}SCN)Mn(NCS)(bipy)_2]_2\}$ and $[Pt(SCN)_4](n\text{-}Bu_4N)_2$, respectively.

Concluding remarks

The absorption and luminescence spectra shown in this overview illustrate the detailed quantitative information revealed by experimental observations combined with simple quantitative models. In order to resolve many challenging chemical questions, these two methods alone are not sufficient and other spectroscopic techniques have to be used in order to advance our knowledge on electronic structure and excited-state properties.

Acknowledgments

First and foremost, my thanks go to all undergraduate, graduate and postdoctoral students for their dedicated work in the group since 1991. Selected publications of their results are given in the references and their names are listed at http://mapageweb.umontreal.ca/reber. I am grateful to faculty colleagues at the Département de chimie, Université de Montréal and to a wide circle of collaborators for their support and friendship. Funding from the Natural Sciences and Engineering Research Council (NSERC) and from a number of other agencies is gratefully acknowledged. I sincerely thank the Canadian Society for Analytical Sciences and Spectroscopy for the 2007 Gerhard Herzberg Award.

References

1. This lecture was presented at the 53rd International Conference on Analytical Sciences and Spectroscopy, held at Trent University, Peterborough (Ontario) in June 2007.
2. F. A. Cotton, G. Wilkinson, Advanced Inorganic Chemistry, Fourth Edition. 1988, p. 619.
3. H. A. Bethe, *Ann. Physik*, **3**, 133 (1929).
4. D. S. McClure, *Sol. Stat. Phys.*, **9**, 399 (1959).
5. F. A. Cotton, *J. Chem. Ed.*, **41**, 466 (1964).
6. A. B. P. Lever, Inorganic Electronic Spectroscopy. 2nd ed.; Elsevier Science Publishers B.V.: Amsterdam, 1984.
7. P. Day, *Angew. Chem. Int. Ed. Engl.* **19**, 290 (1980).
8. J. Ferguson, *Progr. Inorg. Chem.*, **12**, 159 (1970).
9. A. W. Adamson, P. D. Fleischauer, Concepts of Inorganic Photochemistry. Krieger Publishing Company: Malabar, FL, 1984.
10. A. D. Kirk, *Chem. Rev.*, **99**, 1607 (1999).
11. J. I. Zink, *Coord. Chem. Rev.*, **211**, 69 (2001).
12. D. M. Roundhill, J. P. Fackler Jr., Optoelectronic Properties of Inorganic Compounds. Plenum Press: New York and London, 1999.
13. D. R. Gamelin, H. U. Güdel, *Top. Curr. Chem.*, **214**, 1 (2001).
14. H. Riesen, *Coord. Chem. Rev.*, **250**, 1737 (2006).
15. E. J. Heller, R. L. Sundberg, D. Tannor, *J. Phys. Chem.*, **86**, 1822 (1982).
16. W. R. Browne, J. J. McGarvey, *Coord. Chem. Rev.*, **251**, 454 (2007).
17. K.-S. Kim Shin, J. I. Zink, *Inorg. Chem.*, **28**, 4358 (1989).
18. J. I. Zink, K.-S. K. Shin, *Adv. Photochem.*, **16**, 119 (1991).
19. J. Telser, *J. Braz. Chem. Soc.*, **17**, 1501 (2006).
20. C. J. Ballhausen, Introduction to Ligand Field Theory. McGraw-Hill: New York, 1962.
21. S. Sugano, Y. Tanabe, H. Kamimura, Multiplets of Transition Metal Ions in Crystals. Academic Press: New York, London, 1970.
22. C. Reber, R. Beaulac. In Compr. Coord. Chem. II, McCleverty, J. A.; Meyer, T. J., Eds. Elsevier Pergamon: Amsterdam, 2003; Vol. 2, p. 287.
23. E. J. Heller, *Acc. Chem. Res.*, **14**, 368 (1981).
24. T. Brunold, H. U. Güdel. In Inorganic Electronic Structure and Spectroscopy, Solomon, E. I.; Lever, A. B. P., Eds. John Wiley & Sons, Inc.: New York, 1999; Vol. I, p. 259.
25. L. J. Larson, J. I. Zink, *Inorg. Chem.*, **28**, 3519 (1989).
26. L. Tutt, J. I. Zink, *J. Am. Chem. Soc.*, **108**, 5830 (1986).
27. C. Reber, J. Landry-Hum. In Compr. Coord. Chem. II, McCleverty, J. A.; Meyer, T. J., Eds. Elsevier Pergamon: Amsterdam, 2003; Vol. 2, p. 559.
28. S. Masson, M. Triest, C. Reber, *Chem. Educator* **6**, 147 (2001). http://dx.doi.org/10.1333/s00897000466a
29. M. Triest, S. Masson, J. K. Grey, C. Reber, *PhysChemComm*, **3**, 64 (2000). http://dx.doi.org/10.1039/b008386k
30. M. Triest, G. Bussière, H. Bélisle, C. Reber, *J. Chem. Ed.* **77**, 670 (2000). http://jchemed.chem.wisc.edu/JCEWWW/Articles/JCENi/JCENi.html
31. D. Tannor, Introduction to Quantum Mechanics A Time-Dependent Perspective. University Science Books: Sausalito, CA, 2007.
32. F. Gilardoni, J. Weber, K. Bellafrouh, C. Daul, H.-U. Güdel, *J. Chem. Phys.*, **104**, 7624 (1996).
33. J. Landry-Hum, G. Bussière, C. Daniel, C. Reber,

Inorg. Chem., **40**, 2595 (2001).
34. C. Daniel, *Coord. Chem. Rev.*, **230**, 65 (2002).
35. C. Daniel, *Coord. Chem. Rev.*, **238**, 143 (2003).
36. F. Neese, P. Petrenko, D. Ganyushin, G. Olbrich, *Coord. Chem. Rev.*, **251**, 288 (2007).
37. B. Z. Shakhashiri, G. E. Dirreen, F. Juergens, *J. Chem. Ed.*, **57**, 900 (1980).
38. P. O'Brien, *J. Chem. Ed.*, **59**, 1052 (1982).
39. G. Pass, H. Sutcliffe, Practical Inorganic Chemistry, Second Edition. Chapman and Hall Science Paperbacks: London, 1974.
40. G. S. Girolami, T. B. Rauchfuss, R. J. Angelici, Synthesis and Technique in Inorganic Chemistry. University Science Books: Sausalito, CA, 1999.
41. C. Reber, J. I. Zink, *J. Chem. Phys.*, **96**, 2681 (1992).
42. D. Neuhauser, T.-J. Park, J. I. Zink, *Phys. Rev. Lett.*, **85**, 5304 (2000).
43. G. Bussière, C. Reber, D. Neuhauser, D. A. Walter, J. I. Zink, *J. Phys. Chem. A*, **107**, 1258 (2003).
44. M.-C. Nolet, R. Beaulac, A.-M. Boulanger, C. Reber, *Struct. Bond.*, **107**, 145 (2004).
45. M.-C. Nolet, A. Michaud, C. Bain, D. Zargarian, C. Reber, *Photochem. Photobiol.*, **82**, 57 (2006).
46. C. K. Jørgensen, *Acta Chem. Scand.***, 9**, 1362 (1955).
47. A. D. Liehr, C. J. Ballhausen, *Ann. Phys.*, **6**, 134 (1959).
48. M. H. L. Pryce, G. Agnetta, T. Garofano, M. B. Palma-Vittorelli, M. U. Palma, *Phil. Mag.*, **10**, 77 (1964).
49. E. I. Solomon, C. J. Ballhausen, *Mol. Phys.*, **29**, 279 (1975).
50. G. Bussière, C. Reber, *J. Am. Chem. Soc.*, **120**, 6306 (1998).
51. G. Bussière, R. Beaulac, B. Cardinal-David, C. Reber, *Coord. Chem. Rev.***, 219**, 509 (2001).
52. E. González, A. Rodrigue-Witchel, C. Reber, *Coord. Chem. Rev.*, **251**, 351 (2007).
53. R. Beaulac, C. Reber, *Inorg. Chem.,* **47**, 5048 (2008).
54. J. K. Grey, I. S. Butler, C. Reber, *J. Am. Chem. Soc.*, **124**, 11699 (2002).
55. J. K. Grey, I. S. Butler, C. Reber, *Can. J. Chem.*, **82**, 1083 (2004).
56. V. M. Miskowski, H. B. Gray, M. D. Hopkins. In Adv. in Trans. Met. Coord. Chem., Che, C.-M.; Yam, V. W.-W., Eds. JAI Press: Greenwich, CT, 1996; Vol. 1, p. 159.
57. C. Savoie, C. Reber, *J. Am. Chem. Soc.*, **122**, 844 (2000).
58. C. Savoie, C. Reber, *Coord. Chem. Rev.*, **171**, 387 (1998).
59. C. Savoie, C. Reber, S. Bélanger, A. L. Beauchamp, *Inorg. Chem.*, **34**, 3851 (1995).
60. J. R. Winkler, H. B. Gray, *Inorg. Chem.*, **24**, 346 (1985).
61. J. R. Winkler, H. B. Gray, *J. Am. Chem. Soc.,* **105**, 1373 (1983).
62. R. A. Kirgan, B. P. Sullivan, D. P. Rillema, *Top. Curr. Chem.*, **281**, 45 (2007).
63. L. Tutt, D. Tannor, E. J. Heller, J. I. Zink, *Inorg. Chem.*, **21**, 3858 (1982).
64. L. W. Tutt, J. I. Zink, E. J. Heller, *Inorg. Chem.*, **26**, 2158 (1987).
65. J. A. G. Williams, *Top. Curr. Chem.*, **281**, 205 (2007).
66. C. J. Ballhausen, *Theor. Chim. Acta*, **3**, 368 (1965).
67. D. M. Preston, W. Güntner, A. Lechner, G. Gliemann, J. I. Zink, *J. Am. Chem. Soc.*, **110**, 5628 (1988).
68. C. Reber, J. I. Zink, *J. Phys. Chem.*, **95**, 9151 (1991).
69. Y. Pelletier, C. Reber, *Inorg. Chem.*, **39**, 4535 (2000).
70. Y. Pelletier, C. Reber, *Inorg. Chem.*, **36**, 721 (1997).
71. R. W. Parsons, H. G. Drickamer, *J. Chem. Phys.,* **29**, 930 (1958).
72. D. R. Stephens, H. G. Drickamer, *J. Chem. Phys.,* **34**, 937 (1961).
73. H. G. Drickamer, *Sol. Stat. Phys.*, **17**, 1 (1965).
74. K. L. Bray, *Top. Curr. Chem.*, **213**, 1 (2001).
75. J. K. Grey, I. S. Butler, *Coord. Chem. Rev.,* **219**, 713 (2001).
76. C. Reber, J. K. Grey, E. Lanthier, K. A. Frantzen, Comments on *Inorg. Chem.*, **26**, 233 (2005).
77. J. K. Grey, I. S. Butler, C. Reber, *Inorg. Chem.*, **42**, 6503 (2003).
78. J. K. Grey, I. S. Butler, C. Reber, *J. Am. Chem., Soc.* **124**, 9384 (2002).
79. G. Levasseur-Thériault, C. Reber, C. Aronica, D. Luneau, *Inorg. Chem*., **45**, 2379 (2006).